Materials Chemistry and Physics 147 (2014) 744–750

Contents lists available at ScienceDirect

Materials Chemistry and Physics

journal homepage: www.elsevier.com/locate/matchemphys

Synthesis and characterization of conductive copper-based metal-organic framework/graphene-like composites

Michela Alfè [a, *], Valentina Gargiulo [a], Luciana Lisi [a], Roberto Di Capua [b]

[a] Istituto di Ricerche sulla Combustione (IRC) – CNR, P.le Tecchio 80, I-80125 Naples, Italy
[b] Dipartimento di Fisica, Università di Napoli Federico II, and SPIN-CNR UOS Napoli, via Cintia, I-80126 Napoli, Italy

HIGHLIGHTS

- A new class of HKUST-1/graphene-like composites was produced.
- High amount of graphene-like does not interfere with the HKUST-1 crystal growing.
- Composites exhibit a new porosity.
- Strong increase of the dc conductivity as a function of graphene-like content.

GRAPHICAL ABSTRACT

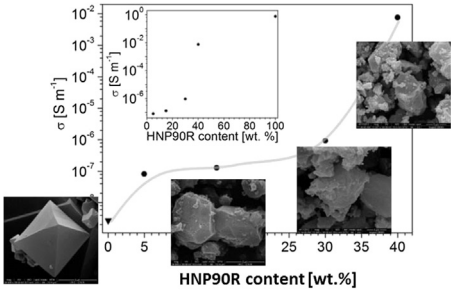

ARTICLE INFO

Article history:
Received 11 January 2014
Received in revised form
29 April 2014
Accepted 9 June 2014
Available online 25 June 2014

Keywords:
Composite materials
Organometallic compounds
Microporous materials
Nanostructures
Electrical characterisation

ABSTRACT

Metal-organic framework (MOF) incorporating conductive graphene-like layers were synthesized and characterized. The selected MOF, HKUST-1, combines high surface area, water stability, simple preparation and low costs. Graphene-like layers incorporated into the MOF structure were obtained by a two-step oxidation/reduction wet treatment of a high surface carbon black. MOF composites were produced at different carbonaceous layers content. It was shown, through a wide characterization of the samples, that the composites preserve the main features of the parent MOF, additional exhibiting a tunable electrical conductivity.

1. Introduction

Metal-organic frameworks (MOF) are coordination networks characterized by a high crystallinity and uniform porosity, obtained by the assembly of metallic centers and organic linkers through strong covalent bonds. MOF attracted in the last years a great attention due to their high surface area (up to 4500 $m^2 g^{-1}$) [1] and the possibility to vary their metallic centers and organic functionalities [2] in order to tune chemico-physical and textural properties for a large array of specific applications. Because of such features (large internal surface area and high porosity and crystallinity) MOF are often compared with zeolites: similarly to zeolites, MOF have been utilized in some applications including adsorption and separation of specific gases [3], gas storage [4–8], heterogeneous catalysis [9] drug delivery [10] and chemical sensors [11]. The principal disadvantages of MOF are the tendency of reversible binding of water, the air- and moisture sensitivity and a lower chemical and thermal stability compared to zeolites

* Corresponding author.
E-mail address: alfe@irc.cnr.it (M. Alfè).

http://dx.doi.org/10.1016/j.matchemphys.2014.06.015
0254-0584/

and other porous inorganic solids [1]. The electrical properties of MOF were very rarely studied due to their insulating nature. The preparation of composites combining MOF and carbon-based materials (carbon nanotubes, CNT [12], graphite oxide, GO [13], graphite [14]) has been proposed as a solution to overcome the weak points of MOF and to expand their field of applications. Studies on a zinc-based MOF (MOF-5) show that MOF-5 intercalated with graphene decorated at the basal plane with carboxylic groups exhibit new electrical properties [15]. These composites combine the properties of carbonaceous surfaces and MOF. The introduction of carbonaceous material into MOF structure potentially leads to an enhancement in non-specific adsorption improving the kinetics of adsorption. Moreover, the conductivity and high specific surface area of graphene can strongly affect the dielectric and conducting properties of host materials, which could fulfill the recently highlighted request for MOF with conducting properties for several applicative purposes [15–16].

This paper focuses on the synthesis and description of the structure of MOF in which conductive graphene-like layers are embedded. We chose a copper-based MOF containing Cu^{2+} dimers as the metallic units linked to oxygen atoms from benzene tricarboxylate (BTC) [17–18], and referred in literature as HKUST-1 or MOF-199. HKUST-1 combines high surface area, water stability [19], simple preparation (anhydrous conditions are not required) and low costs (precursors are easily available and not expensive). Graphene-like layers used to prepare the composites were obtained by a two-step oxidation/reduction wet treatment of a high surface carbon black (CB), according to the procedure described in Alfè et al. [20]. This procedure offers high reproducibility and control of the results and it is extremely inexpensive. In this work we show, through a wide characterization of samples with several carbonaceous layers content, that the obtained composites preserve the main features of the parent MOF, additionally exhibiting a tunable electrical conductivity.

2. Experimental section

2.1. Sample preparation

HKUST-1 preparation. The MOF HKUST-1 was prepared applying the synthetic procedure reported by Petit[13]: 1 g of copper nitrate hemipentahydrate and 0.5 g of 1,3,5 benzenetricarboxylic acid (BTC, 0.5 g) were mixed in 8.5 mL of *N*,*N* dimethylformamide (DMF) under stirring and sonication (5 min). 8.5 mL of ethanol were then added to the mixture, which was stirred and sonicated 5 min more. Finally, 8.5 mL of deionized water were added too and the mixture was kept under stirring and sonication for 30 min. The mixture was then heated at 85 °C for 21 h under stirring. After cooling, the crystals were recovered by filtration, washed and immersed in dichloromethane for three days and finally collected by filtration. All chemicals were purchased from Sigma–Aldrich of the purest quality and used without further purification.

Graphene-like (GL) layers preparation. GL layers in water suspension were prepared according to a two-step procedure proposed in Alfè et al. [20]. Briefly, CB (Phillips Petroleum Co., furnace carbon black, 15–20 nm primary particles diameter, specific BET area 151 $m^2\ g^{-1}$) was oxidized with nitric acid (67%) at 100 °C under stirring for 90 h. The oxidized carbon nanoparticles were recovered by centrifugation and named HNP90. The product had a dark brown appearance and it was not as opaque black as the pristine CB. The HNP90 was dispersed in water and treated with hydrazine hydrate (50%) at 100 °C under reflux for 24 h. At the end of the reaction the excess of hydrazine was neutralized with nitric acid and the resulting black solid recovered by centrifugation and named HNP90R. The HNP90R mass yield was 55%. It is noteworthy that the dried HNP90R resulted to be insoluble in water and in the most common organic solvents, both polar and apolar (water, ethanol, *N*-methyl pirrolidinone, dichloromethane, heptane, DMF) [20]. This was attributed to an increase of hydrophobicity of the material caused by a decrease in the polar functionalities on the surface and consequent intimate self-assembling interaction between the restored graphitic planes leading to the formation of a graphene-like assembling. For this reason freshly prepared HNP90R in water suspension was readily used for the preparation of the composites.

MOF/GL (MGL) preparation. HNP90R suspension was added to the well-dissolved MOF precursors and solvent mixture during the final step of the MOF preparation, in substitution of the volume of deionized water. The synthesis conditions were kept the same as those used for the preparation of the HKUST-1. Four MGL composites were prepared with a different HNP90R loading and named MGL-1, MGL-2, MGL-3 MGL-4 (5, 15, 30, 40 wt.% of HNP90R, respectively). In all cases the liquid phase recovered after the filtration of the crystals resulted colorless, indicating a complete incorporation of the GL material into the MOF structure. The percentage of the incorporated GL was checked by elemental analysis and inductively coupled plasma mass spectrometry (ICP-MS).

2.2. Methods

Elemental composition of the samples (C, H, N) was estimated by a Perkin–Elmer 2400 CHNSO elemental analyzer. The quantitative determination of the Cu was obtained by an Agilent ICP-MS 7500ce spectrometer. For the ICP-MS measurements, 50 mg of the powdered sample was suspended with 5 mL of deionized water and digested with 5 mL of HNO_3 (65%) and 1 mL of H_2O_2 (30%) for 30 min by microwave heating. The digested sample was filtered to remove any particulate or solid contaminant which may interfere with the analysis, diluted with deionized water and analyzed. The quantitative determination of copper was achieved extrapolating from a four point calibration curve. Each measurement was repeated thrice.

The thermal stability of the samples was evaluated by thermogravimetric analysis (TGA) on a Perkin–Elmer Pyris 1 Thermogravimetric Analyzer. The samples were heated both in oxidant (air) and in inert (nitrogen) environment (30 mL min^{-1}) from 30 °C up to 750 °C at a rate of 10 °C min^{-1}.

Fourier Transform Infrared (FTIR) spectra were recorded on a Nicolet iS10 spectrometer using the attenuated total reflectance (ATR) method by using a germanium crystal. The spectra were acquired on the powdered samples without KBr addition.

BET specific surface area and pore size distribution of the samples were evaluated using a Quantachrome Autosorb 1-C by Ar adsorption at 87 K in order to limit the p/p_0 range in comparison to N_2, requiring lower p/p_0 value for adsorption into micropores [21]. The samples were outgassed under vacuum at 110 °C before the analysis. Data of the adsorption branch of the complete isotherm were processed according to NLDFT method to evaluate the pore size distribution and pore volume.

X-ray diffraction (XRD) analyses were carried out using a Philips PW1710 diffractometer operating between 5°2θ and 60°2θ with a Cu Kα radiation ($\lambda = 1.54056$ Å). The sample powder was grounded and then loaded into a glass holder and leveled with a glass slide before mounting it on the sample chamber. A diffraction experiment was run on standard glass slide for the background correction.

Scanning electron microscopy (SEM) was performed on a FEI Inspect™ S50 Scanning Electron Microscope. SEM was performed

on the powdered sample, previously dried and sputter coated with a thin layer of gold to avoid charging.

Basic electrical characterization shows the effect of the reduction on the transport properties. The electrical dc conductivity was measured in a four contact geometry (low currents recorded through a Keithley picoammeter model 6485). The measurements were carried out on samples obtained by compacting the powder in a compression setup. A pellet of 1 cm diameter with a polished mirror-like surface was obtained at a compacting pressure of 5 atm. The thickness of each pellet was estimated by SEM images and it was found to be in the range of 100–200 μm height. Experiments for each material were carried out in triplicate and characterized by a reproducibility of 10%.

3. Results and discussion

Table 1 reports the elemental composition of the four MGL composites together with the pure MOF and HNP90R. The oxygen amount was evaluated by difference. The elemental analyses of the HNP90R precursors (CB and HNP90) are reported elsewhere [20]. Elemental analysis indicates that the oxygenated functionalities in HNP90R are not completely removed upon the chemical reduction step, leading to an oxygen content quantifiable as 39.61 wt. %. The presence of nitrogen (likely in the form of nitrogroups or hydrazones) is also observed (6.09 wt. %). The O/C atomic ratio is 0.56 (comparable to the graphene layers obtained from the reduction of GO by hydrazine [22]) and the number of surface acidic site content (performed applying a sensitive and fast fluorimetric assay with thionin acetate [20]) is 1.7×10^{-7} molCOOH mg^{-1}.

The measured values of C, H, Cu and N in the composites were compared with the "hypothetical" ones, calculated combining the fraction of HNP90R and HKUST-1 in the composite with the percentages of each element in HNP90R and HKUST-1 according with the following equation:

$$X_{tot} = X_{HNP90R} \times f_{HNP90R} + X_{HKUST\text{-}1} \times f_{HKUST\text{-}1}$$

where X_{tot} (X = C, O, H, Cu, or N) is the element percentage in the composite (expressed as wt. %), X_{HNP90R} and $X_{HKUST\text{-}1}$ are the percentage (wt. %) of the same element in HNP90R and HKUST-1 respectively, and f_{HNP90R} and $f_{HKUST\text{-}1}$ are the weight fractions of HNP90R and HKUST-1 in the composite ($f_{HKUST\text{-}1} = 1 - f_{HNP90R}$). The good accordance between the measured and the "hypothetical" values is a good indication of a complete incorporation of the carbonaceous layers into the composite. Trends are provided as supplementary info.

Fig. 1 reports the XRD patterns of the parent materials as well as the composites. In the case of HNP90R, a single broad peak around 2θ 23° is observed. The MOF diffraction pattern is in accordance with those reported in the literature for HKUST-1 [17,23]. Although the agreement with the HKUST-1 X-ray diffraction pattern [17] is quite good, deviations in the relative intensity (i.e. the peak at 2θ = ~6–7° due to the (111) reflection) are attributable to variations in the degree of hydration, as reported in Ref. [24]. The HKUST-1 diffraction pattern is similar to the composites revealing the existence of the well-defined MOF units in the composites themselves. This indicates that the presence of HNP90R in the reaction mixture does not prevent the formation of linkages between Cu ions and the BTC molecules, leading to the formation of HKUST-1 crystals. Besides the high degree of crystallinity that can be inferred by the sharp HKUST-1 diffraction peaks, the pattern also indicates a negligible presence of the competing Cu_2O phase, whose characteristic 2θ peaks (around 36° and 43°) are extremely weak or even absent.

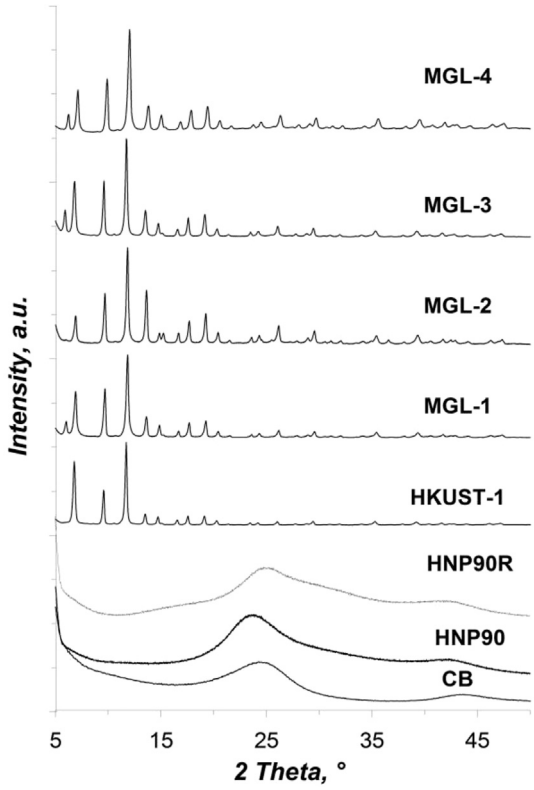

Fig. 1. XRD patterns of the parent materials and the MGL composites.

The SEM images, reported in Fig. 2, provide information about HKUST-1 and MGL microstructure. Our HKUST-1 sample exhibits typical octahedral crystals [23] of different sizes, with relatively smooth surface. This ensures a high morphological and crystalline quality of the HKUST-1 sample, and makes us confident that the observed different features on the realized MGL composites can be ascribed to the new built structures. In MGL-1 (corresponding to 5 wt.% of incorporated HNP90R), crystals of octahedral shape are still observable. With the increasing quantity of HNP90R in the composites, the octahedral shape characteristic of the HKUST-1 crystal tends to disappear and or to be partially hidden by some different formations. In the case of the MGL-4 (40 wt.% of HNP90R loading), small agglomerates are observable in which the octahedral shape of the pristine HKUST-1 crystal is not clearly discernible. The sharp XRD pattern still indicates crystal order in this sample: it is therefore not easy to understand if the small observed agglomerates are mainly due to small HKUST-1 crystals or to some spurious phases (which from XRD measurements seem to be still a

Table 1
Samples composition. "Hypothetical" composition of the composites is reported in the brackets.

Sample	HNP90R amount wt.%	Elemental composition				
		C wt.%	O wt.%	H wt.%	Cu wt.%	N wt.%
HKUST-1	0	26.64	34.69	2.45	35.7	0.52
HNP90R	100	52.9	39.61	1.4	0	6.09
MGL-1	5	29.64	31.19	2.47	35.5	1.2
		(27.95)	(39.3)	(2.39)	(33.9)	(0.80)
MGL-2	15	32.07	29.05	2.01	35.1	1.77
		(30.6)	(38.8)	(2.29)	(30.3)	(1.35)
MGL-3	30	38.33	32.51	2.03	24.4	2.73
		(34.5)	(38.1)	(2.13)	(24.9)	(2.19)
MGL-4	40	39.22	33.38	1.65	22.7	3.05
		(37.1)	(37.6)	(2.03)	(21.4)	(2.75)

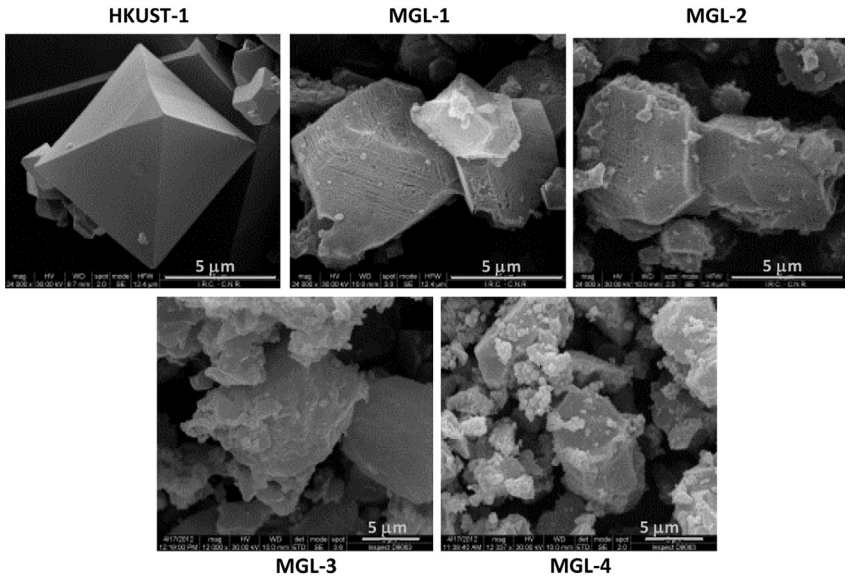

Fig. 2. SEM images of the HKUST-1 and the MGL composites.

minority in MGL-4). It must be noticed that the SEM images did not reveal the typical Cu_2O formations reported in Biemmi et al. [23], consistently with the XRD pattern features. Moreover elemental mapping analysis (EDX) evidenced a chemical uniformity on a large area (Supporting info).

The surface of the composites seems to be affected by the presence of HNP90R. SEM imaging of the composites shows "lace-like" arrangement in the vicinity of the carbonaceous layers embedded within HKUST-1 crystals, similar to those observed by Zhao et al. [25].

The pH of a sample suspension was measured in order to provide information about the acidity and basicity of the surface. About 10 mg of the pure HKUST-1 and composites has been added to 2 mL of distilled water. The suspension has been stirred for 30 min to reach equilibrium before recording the pH. In all cases pH is about 4.15 indicating that, although a morphological effect is evidenced, the incorporation of HNP90R does not alter the surface chemistry of the HKUST-1.

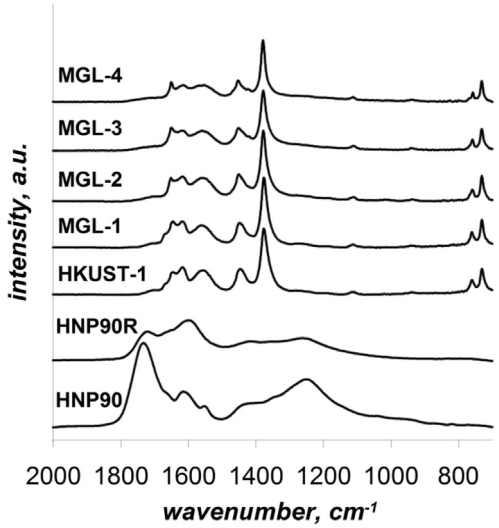

Fig. 3. ATR-IR spectra of the parent materials and the MGL composites.

The ATR-IR spectra of the parent materials and the composites are plotted in Fig. 3 in the 2000–700 cm^{-1} wavenumber region. Spectra are baseline corrected and shifted for clarity. The HNP90 and HNP90R highly conjugated p-network caused peak broadening in the ATR-IR spectra due to the overlapping of several vibration in the 1000–1500 cm^{-1} range [26]. Both spectra exhibit bands at 1750–1650 cm^{-1} (C═O stretching vibrations from carbonyl and carboxylic groups) and 1600–1500 cm^{-1} (skeletal vibration of the sp^2 graphitic domains). The HNP90 spectrum presents an enhanced broad band in the 1300–1100 cm^{-1} region ascribable to the overlapping of C–OH and C–O stretching vibrations. The intensity of the C═O band and of the C═O broad band are significantly weaker in the HNP90R as a consequence of the partial removal of carboxylic–carbonylic functionalities upon the reductive treatment. The spectrum of HKUST-1 is quite similar to those reported in literature [13,27]. The bands at 1645 and 1590 cm^{-1} and at 1450 and 1370 cm^{-1} correspond to the asymmetric and symmetric stretching vibrations of the carboxylate groups in BTC, respectively. In agreement with the XRD data, the ATR-IR spectra of the composites exhibit features similar to the HKUST-1 spectrum. The absence of the C═O bands in the composites ATR-IR spectra suggests that the carboxylic functionalities of the HNP90R have interacted with the copper dimers and chemical interactions are involved in the formation of the composites. It can be speculated that the presence of residual carboxylic groups, located at the edges of the graphene-like basal planes, helps the interaction with the MOF crystals, similarly with those observed for MOF/GO composites [13]. Interestingly, this seems to not interfere with the MOF crystal formation, as shown by XRD investigation (Fig. 1).

The TGA profiles obtained in inert environment (nitrogen) for HNP90R, HKUST-1 and the composites are reported in Fig. 4a. In the case of HNP90R a slow weight loss (~40% of total weight loss) is observable and it is consistent with the progressive decomposition of oxygenated functionalities (carbonylic/carboxylic). The TGA curves of HKUST-1 and the composites exhibit a high weight loss at 300–350 °C corresponding to the collapse of the structure accompanied by the release of CO_2 [13,27]. The behavior of the composites resembles that observed for HKUST-1 indicating a good dispersion of the HNP90R into the composite, confirming the indications coming from the previous characterizations.

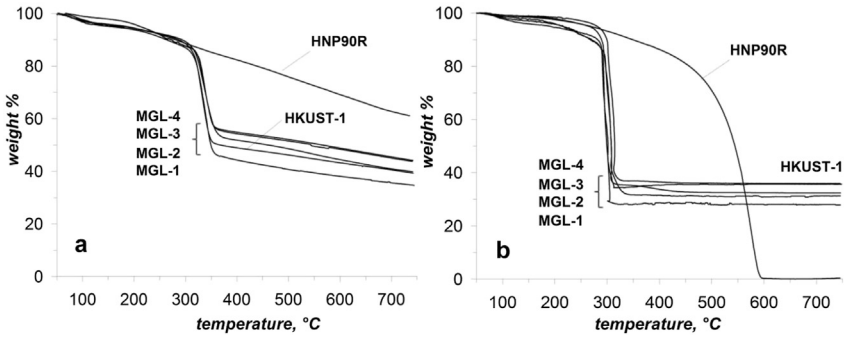

Fig. 4. Thermal analyses of the parent material and the composites in inert (nitrogen, a) and in oxidative environment (b).

As concerns the TGA profiles in oxidative environment (Fig. 4b), on HKUST-1 and on the composites the trend is qualitatively similar to those observed in inert environment. In the case of HNP90R, the TGA curve shows two main weight losses between 150 and 500 °C (20–40% weight loss) and 550 °C (bulk oxidation of HNP90R graphitic core).

Interestingly, the absence of weight loss after 300 °C even for composites with a high load of HNP90R suggests that the Cu ion coordinated with the HNP90R catalyzed the HNP90R oxidation causing the HNP90R to react at temperatures lower than the parent material. This behavior represents a further indication that the HNP90R is well-mixed within the composite. If the composites were a physical mixture of two non-interacting components (HKUST-1 and HNP90R) they would behave in a quite different way after progressive heating in oxidative environment. TGA was performed on 'real' physical mixtures of two components built by mixing at the appropriate % wt. the two pure components. TGA present a distinct weight drop around 500 °C attributed to the combustion of HNP90R component (Supporting info). The absence of such weight drop in the composites, even at a high HNP90R load, indicates a good incorporation of HNP90R into the composites.

In Table 2 the values of BET surface area and the pore volume evaluated from Ar adsorption isotherms are reported. "Hypothetical" values of the BET surface area of the composites, calculated according to a weighted average of the two components, are reported in the brackets.

HKUST-1 has a BET surface area of 1989 $m^2\ g^{-1}$, comparable to the values reported in the literature [1,13] whereas pure HNP90R exhibits a lower surface area (76 $m^2\ g^{-1}$). In the composites both surface area and pore volume decrease with the progressive incorporation of HNP90R. A considerable lower reduction of BET area is observed with respect to a weighted average of the two components (Table 2) indicating non-additive effects due to the incorporation of the HNP90R component. Moreover the analysis of the values of BET surface area suggests that after the first incorporation of HNP90R into HKUST-1 in a low amount (5%wt.) a dramatic reduction of surface area occurs. Further incorporation of HNP90R causes a reduction of the surface area roughly proportional to the fraction of HNP90R indicating that a small fraction of HNP90R is sufficient to modify the HKUST-1 structure, creating a new kind of porosity at the interface between the HNP90R and MOF components.

Table 2
BET surface area and pore volume (from Ar adsorption isotherms) of the parent materials and the composites. "Hypothetical" values of the BET surface area of the composites are reported in the brackets.

Sample	BET area ($m^2\ g^{-1}$)	Pore volume ($cm^3\ g^{-1}$)
HKUST-1	1989	0.98
MGL-1	906 (1893.35)	0.74
MGL-2	709 (1702.05)	0.67
MGL-3	582 (1415.1)	0.62
MGL-4	570 (1223.8)	0.45

In Fig. 5 the Ar adsorption/desorption isotherms of the parent material and the composites are reported. All curves are type I isotherms typically associated to microporous materials; however, a small hysteresis accounts for the presence of some mesopores which tend to decrease in the samples with HNP90R incorporation. This is in agreement with Petit et al. [13] who also observed a more pronounced hysteresis loop for HKUST-1, which decreases by increasing the incorporation level.

The data were processed according to NLDFT method which allows an accurate analysis over the complete micro and mesopore size range in contrast with macroscopic thermodynamic approaches or semi-empirical methods which do not provide a good description of micropore filling [28]. A zeolite/silica model was used to evaluate the pore size distribution and volume. This adsorption model provided the best fitting (fitting error always <0.5%) assuming spherical/cylindrical pores [29]. In Fig. 6 the pore size distribution of the HKUST-1 is compared to that of the composites: the size distributions reflect the lower average size of the pores in composites than in the pure HKUST-1.

The HKUST-1 sample exhibits a typical bimodal micropores distribution with maxima centered at about 5 and 7 Å. This pore structure is altered by even a small fraction of intercalated HNP90R (5% wt.) causing the arise of a new kind of porosity at about 6 Å. This new porosity is likely due to the interaction between the residual carboxylic functionalities of the HNP90R and the copper dimers. Nevertheless, MGL-4 sample surprisingly shows a pore structure distribution more similar to the original material although less definite. This trend can be interpreted as a saturation of the accessible sites on HKUST-1 due to the high amount of HNP90R (40% wt.). The high percentage of HNP90R causes a collapse of the BET surface area (570 $m^2\ g^{-1}$, Table 2) probably due to a HNP90R partial agglomeration that prevents the formation of the porosity centered at 6 Å, exhibited by the composites produced with at a lower HNP90R loading. Similar behavior is reported for GO/HKUST-1 composites [13] whereas the excess of the organic intercalant (GO) tends to restack together, decreasing the overall porosity and preventing the instauration of different kind of porosity due to the interaction between MOF crystals and GO oxygenated functionalities, as in the case of GO/HKUST-1 composites with a lower GO loading. In addition to micropores, representing the dominant type of pores, all materials also show some mesopores in the region 40–60 Å and a few larger pores around 160 Å. The mesopores contribution is quantitatively less significant (about 20% total pore volume) for HKUST-1 sample whereas accounting for 40–60% total pore volume for MGL materials roughly

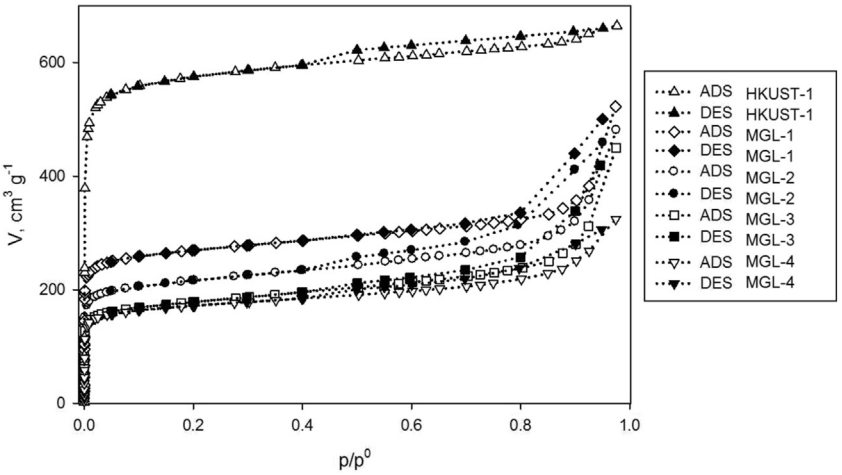

Fig. 5. Ar adsorption/desorption isotherms of the parent material and the MGL composites.

proportionally to the fraction of HNP90R in the material. In other words, the micropore volume, strictly related to the fraction of HKUST-1, decreases with HNP90R incorporation, the mesopores volume being quite constant.

The electrical dc conductivity or resistivity of HKUST-1 and MGL is a useful macroscopic characteristic for a preliminary comparative analysis on the transport properties, since it is governed by both the microstructures and chemical composition. The electrical properties of HKUST-1 are very rarely studied due to its insulating nature: we performed such measurements (evaluating the electrical resistivity according to the Van der Pauw method [30]) in order to understand a possible effect or trend due to HNP90R incorporation.

On HPN90R sample we measured a dc resistivity of about 1.3 Ω m (corresponding to a conductivity of 0.77 S m^{-1}), while the evaluated sheet resistance and bulk resistivity reveal a substantially insulating character as concerns the pristine HKUST-1. As concerns the composites, the electrical conductivity rapidly increases with the added graphene-like percentage (Fig. 7), ranging over 5 orders of magnitude when the HNP90R amounts changes between 5% and 40% wt. The increase does not follow a linear behavior: our estimations indicate a conductivity of the order of 10^{-7} Sm^{-1} when the graphene-like percentage is 5% or 15%, increasing about ten times at 30% wt. of HNP90R content, and becoming 10^{-2} Sm^{-1} when the graphene-like percentage is 40%. So large variations were reported also in experiments with CB filling polymeric or epoxy matrices, leading to a conductivity increasing up to 10 order of magnitudes for filling percentage of the order of 10% or less [31–33]. An increasing trend so strongly superlinear with doping is usually interpreted under percolation theory. Some models, based on 2D/3D network description, bond percolation, or statistical/geometrical properties of mixtures [33–35], applied to insulating matrices filled with conducting microstructures, demonstrate that a slight increase of electrical conductivity should be observed at low doping, and then, increasing the amount of the filling materials, a critical threshold is expected (corresponding to a full percolating path) for the doping level, above which the conductivity should exhibit a sudden increase. The threshold percentage strongly depends on the specific features of the compounds under investigation; our results resemble this general behavior, and the threshold seems to stand around 20%. For higher filling levels, a saturation trend of the electrical conductivity should take place (corresponding to a complete filling of the available sites in the host matrix), in a characteristic S-shaped curve. The MGL composites did not show saturation up to the highest investigated concentration of HNP90R. However, extrapolating the pure HNP90R as an indication of a hypothetic 100% filled composite, the resulting plot (inset in Fig. 7) seems to indicate a possible saturation occurring at HNP90R content not yet investigated. The relatively large threshold and saturation values for the HNP90R concentration (compared to the ones reported in the mentioned works) suggest a weak interaction between the filler particles inside the matrices, probably due to a good dispersion triggered by the high porosity of the host material [33]. This point surely deserves further investigation, and its

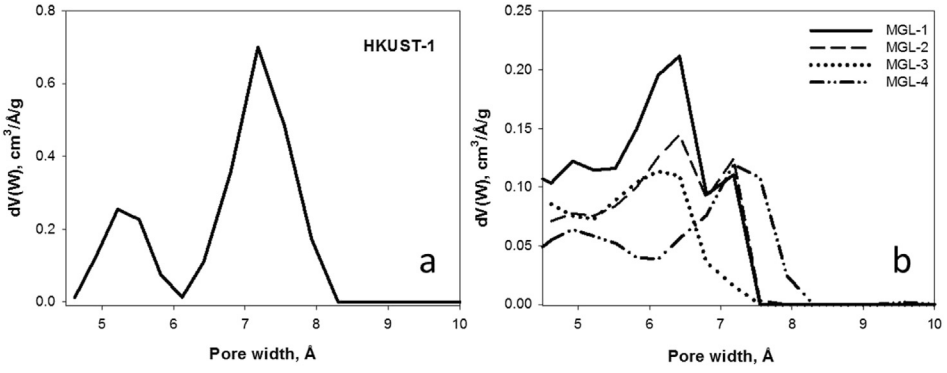

Fig. 6. Pore size distribution of the HKUST-1 (a) and MGL composites (b).

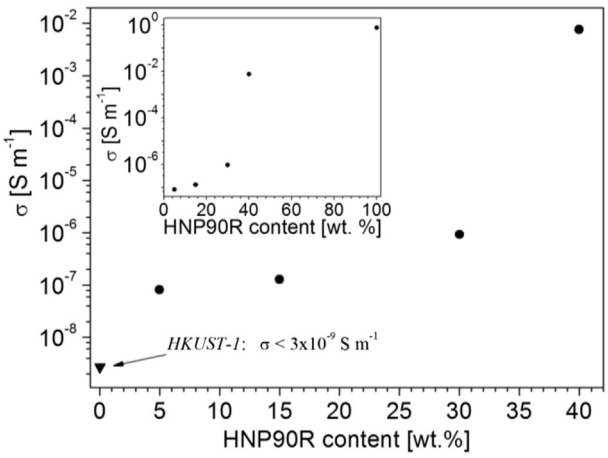

Fig. 7. Electrical conductivity of HKUST-1 and MGL composites.

detailed analysis and discussion are beyond the purposes of the present experimental work.

4. Conclusions

A new class of copper-based metal-organic framework/graphene-like composites were produced starting from the HKUST-1 metal-organic framework. The composites were produced by varying the graphene-like loading and were characterized by XRD and FTIR spectroscopy, TGA, SEM, BET specific surface area and elemental analysis. It was found that the main features of HKUST-1 in the composites are preserved, indicating that the interaction of the HKUST-1 units with the carboxylic functionalities of HNP90R does not interfere with the HKUST-1 crystal growing. It was shown that the incorporation of HNP90R introduces a new porosity in the composites although the surface area of the composites is lower than the HKUST-1 suggesting a distortion in the porous structure of the materials. Preliminary electrical measurements revealed a strong increase of the dc conductivity in the samples as a function of HNP90R content. The conductivity and the new porosity distribution arising by graphene-like incorporation, together with high specific surface area of the composites, can impart new properties to the pristine HKUST-1. The production of electrically conducting porous phases would be of great interest for possible applications in molecular sensing and selective electrode materials as well as proton exchange membrane fuel cells: the indication of tunable electrical conductivity while the remaining features of the parent HKUST-1 are left substantially untouched opens the perspectives for developing such applications.

Acknowledgment

This work was financially supported by the Accordo CNR-MSE “Utilizzo pulito dei combustibili fossili ai fini del risparmio energetico” 2011–2012. The authors also acknowledge Luciano Cortese (XRD analyses and SEM imaging) and Fernando Stanzione (ICP-MS analyses).

Appendix A. Supplementary data

Supplementary data related to this article can be found at http://dx.doi.org/10.1016/j.matchemphys.2014.06.015.

References

[1] N. Stock, S. Biswas, Chem. Rev. 112 (2012) 933–969.
[2] H. Chae, D. Siberio-Perez, J. Kim, Y. Go, M. Eddaoudi, A. Matzger, M. O'Keeffe, O.M. Yaghi, Nature 427 (2004) 523–527.
[3] J. Liu, P.K. Thallapally, B.P. McGrail, D.R. Brown, Chem. Soc. Rev. 41 (2012) 2308–2322.
[4] N.A. Khan, Z. Hasan, S.H.J. Jhung, Hazard. Mater. 244–245 (2013) 444–456.
[5] K. Sumida, D.L. Rogow, J.A. Mason, T.M. McDonald, E.D. Bloch, Z.R. Herm, T.-H. Bae, J.R. Long, Chem. Rev. 112 (2012) 724–781.
[6] J.R. Li, Y. Ma, M.C. McCarthy, J. Sculley, J. Yu, H.K. Jeong, P.B. Balbuena, H.-C. Zhou, Coord. Chem. Rev. 255 (2011) 1791–1823.
[7] J.R. Li, J. Sculley, H.C. Zhou, Chem. Rev. 112 (2012) 869–932.
[8] M.P. Suh, H.J. Park, T.K. Prasad, D.W. Lim, Chem. Rev. 112 (2012) 782–835.
[9] M. Ranocchiari, J.A. van Bokhoven, Phys. Chem. Chem. Phys. 13 (2011) 6388–6396.
[10] P. Horcajada, R. Gref, T. Baati, P.K. Allan, G. Maurin, P. Couvreur, G. Férey, R.E. Morris, C. Serre, Chem. Rev. 112 (2012) 1232–1268.
[11] S. Achmann, G. Hagen, J. Kita, I.M. Malkowsky, C. Kiener, R. Moos, Sensors 9 (2009) 1574–1589.
[12] S.J. Yang, J.Y. Choi, H.K. Chae, J.H. Cho, K.S. Nahm, C.R. Park, Chem. Mater. 21 (2009) 1893–1897.
[13] C. Petit, J. Burress, T.J. Bandosz, Carbon 49 (2011) 563–572.
[14] C. Petit, B. Mendoza, D. O'Donnell, T.J. Bandosz, Langmuir 27 (2011) 10234–10242.
[15] M. Jahan, Q. Bao, J.X. Yang, K.P. Loh, J. Am. Chem. Soc. 132 (2010) 14487–14495.
[16] C.H. Hendon, D. Tiana, A. Walsh, Phys. Chem. Chem. Phys. 14 (2012) 13120–13132.
[17] S.S.Y. Chui, S.M.F. Lo, J.P.H. Charmant, A.G. Orpen, I.D. Williams, Science 283 (1999) 1148–1150.
[18] C. Prestipino, L. Regli, J.G. Vitillo, F. Bonino, A. Damin, C. Lamberti, Chem. Mater. 18 (2006) 1337–1346.
[19] J.J. Low, A.I. Benin, P. Jakubczak, J.F. Abrahamian, S.A. Faheem, R.R. Willis, J. Am. Chem. Soc. 131 (2009) 15834–15842.
[20] M. Alfè, V. Gargiulo, R. Di Capua, F. Chiarella, J.-N. Rouzaud, A. Vergara, A. Ciajolo, ACS Appl. Mater. Interfaces 4 (9) (2012) 4491–4498.
[21] J. Jagiello, M. Thommes, Carbon 42 (7) (2004) 1225–1229.
[22] S. Stankovich, R.D. Piner, S.T. Nguyen, R.S. Ruoff, Carbon 44 (2006) 3342–3347.
[23] E. Biemmi, S. Christian, N. Stock, T. Bein, Micropor. Mesopor. Mater. 117 (1–2) (2009) 111–117.
[24] K. Schlichte, T. Kratzke, S. Kaskel, Micropor. Mesopor. Mater. 73 (2004) 81–88.
[25] Y. Zhao, M. Seredych, Q. Zhong, T.J. Bandosz, ACS Appl. Mater. Interfaces 5 (2013) 4951–4959.
[26] A. Santamaria, N. Yang, E. Eddings, F. Mondragon, Combust. Flame 157 (2010) 33–42.
[27] Y.K. Seo, G. Hundal, I.T. Jang, Y.K. Hwang, C.H. Jun, J.S. Chang, Micropor. Mesopor. Mater. 119 (1–3) (2009) 331–337.
[28] S. Lowell, J.E. Shields, M.A. Thomas, M. Thommes, in: Micropore Analysis, Kluwer Academic Press, 2004.
[29] P.I. Ravikovitch, A. Vishnyakov, A.V. Neimark, Phys. Rev. E 64 (2001) 011602, 1–20.
[30] L. Van der Pauw, J. Philips, Res. Rep. 13 (1958) 1–9.
[31] J.C. Huang, C.L. Wu, Adv. Polym. Technol. 19 (2000) 132–139.
[32] Y. Chekanov, R. Ohnogi, S. Asai, M. Sumita, J. Mater. Sci. 34 (1999) 5589–5592.
[33] J.-C. Huang, Adv. Polym. Technol. 21 (2002) 299–313.
[34] S. Kikrpatrick, Rev. Mod. Phys. 4 (1973) 574–588.
[35] F. Lux, J. Mater. Sci. 28 (1993) 285–301.